Two-quasiparticle-plus-rotor bandmixing calculations of Coriolis decoupling

C. Flaum* and D. Cline
Nuclear Structure Research Laboratory,† University of Rochester, Rochester, New York 14627
(Received 6 November 1975)

Two-quasiparticle-plus-rotor bandmixing calculations have been performed to ascertain whether they can reproduce the phenomena of backbending and anomalous negative parity bands which have been observed in several even-even nuclei. The consequences of this model are discussed in detail for ^{156}Er and some results for ^{104}Pd are presented. The calculations reproduce the observed spectra and electromagnetic decay properties demonstrating the importance of the Stephens and Simon decoupling model. A new coupling scheme clearly emerges, for high-spin two-quasiparticle states at intermediate deformation, where both the magnitude of the intrinsic spin of the particles and its projection on the axis of rotation are approximately good quantum numbers. The residual two-quasiparticle interaction has been shown to have little influence on the high-spin behavior.

[NUCLEAR STRUCTURE ^{156}Er and ^{104}Pd; calculated E_x, wave functions, and electromagnetic properties of two-quasiparticle bands; demonstrated the applicability of the Coriolis decoupling model.]

I. INTRODUCTION

One intriguing result of recent studies of high-spin states in nuclei has been the discovery[1] of the anomalous behavior of the nuclear moment of inertia at high spin, commonly called "backbending."[2-4] This dramatic deviation from simple rotational behavior stimulated an intensive theoretical investigation of this phenomenon.[5-8] Experimental evidence strongly suggests that backbending is a manifestation of the intersection of the ground state band with another rotational band which possesses a larger moment of inertia. Coriolis antipairing[5] and Coriolis decoupling[6] have emerged as the two mechanisms most likely to produce the band intersecting the ground state band.

The moment of inertia in nuclei is about half the rigid rotor value due to the presence of the pairing interaction. Mottelson and Valatin[5] proposed that the Coriolis force could cause a sudden phase transition at sufficiently high angular momentum, resulting in a sudden increase in the moment of inertia, that is, the Coriolis antipairing mechanism. This is analogous to the superconducting to normal phase transition which occurs for a superconductor in a magnetic field, i.e., the Meissner effect. However, it is not clear that an exact analogy with a superconductor can be made. Electrons in a superconductor move in a highly degenerate conduction band, and superconducting properties depend strongly on this degeneracy. In a nucleus, however, the nucleons are bound in single-particle orbits separated from each other by energies comparable to the pairing energies, making the possibility of a sudden coherent pairing breakdown less likely. It is equally probable that only one or two pairs are broken at a time.

Stephens and Simon[6] attributed the observed backbending to the intersection of the ground state rotational band with a Coriolis decoupled rotational band based on states for which only one pair of nucleons is broken, i.e., the so-called two-quasiparticle (2qp) states. The Coriolis force favors alignment of the angular momentum of the unpaired nucleons along the axis of rotation. Coriolis decoupling is a well known phenomenon[9] in odd-A nuclei and the decoupling is particularly large for particles in high j, low Ω orbitals where the Coriolis matrix elements are largest. The strength of the Coriolis force increases with increasing spin and may be sufficient to depress the high-spin members of the decoupled two-quasiparticle rotational bend below the zero-quasiparticle ground state rotational band. The moment of inertia of the yrast states (lowest energy state for each spin and parity) will then indicate an anomaly at the spin value where the decoupled two-quasiparticle band intersects the zero-quasiparticle ground state band. Recent evidence[10,11] supports this Coriolis decoupling picture.

The original paper of Stephens and Simon[6] on backbending in rare earth nuclei attributed the observed backbending to decoupled two-quasineutron configurations in the low Ω $i_{13/2}$ orbitals. It is natural to expect similar behavior for particles in other high-j orbitals. In addition, negative-parity decoupled two-quasiparticle bands are expected to occur at similar energies to the positive-parity two-quasiparticle bands. In fact, negative-parity decoupled bands and extreme backbending have been observed[10] in ^{126,128}Ba even though the $i_{13/2}$ orbital is not active for these nuclei. This ob-

servation prompted us to make a quantitative comparison of the barium data with the predictions of the Coriolis decoupling model and remarkably good agreement was obtained.[10,29] This model explained both the positive- and negative-parity bands in addition to known isomeric states.[12] Similar positive and negative decoupled band behavior appears to occur[13,14] in ^{104}Pd and ^{156}Er, suggesting that Coriolis decoupling may be an important phenomenon in many nuclei. The purpose of the present paper is to show that the two-quaisparticle plus-rotor model can quantitatively reproduce the observed decoupled band behavior in ^{156}Er and ^{104}Pd without resort to detailed parameter searching, and to study the consequences of this model.

Although both the Stephens and Simon[6] (SS) and the present calculations are based on the same model, the two calculations differ in the following respects. (1) The present calculations consider both positive- and negative-parity bands based on both protons and neutrons in several shells in contrast to SS, who concentrate on positive-parity bands due to neutrons in the $i_{13/2}$ orbit. (2) Configurations based on the most important five to eight Nilsson orbitals closest to the Fermi level were included in the present calculation. In contrast, SS restricted their calculations to all seven Nilsson orbitals based on the $i_{13/2}$ neutron orbit. The present truncation scheme is most appropriate when Coriolis decoupling is incomplete, i.e., for states with $I \leq 20$. These are the conditions applicable to the present discussion. The SS truncation scheme works best for extremely high spins when the Coriolis decoupling is almost complete. (3) The interaction between the two-quasiparticle (2qp), 0qp, and 4qp states is very weak, therefore only 2qp configurations were considered explicitly in the present calculations. The 0qp, 2qp, and 4qp states were explicitly included by SS (4) A variable moment of inertia taken from the ground state band was used in the present calculations to compensate for Coriolis antipairing effects. A fixed moment of inertia was used by SS. (5) The influence of the residual 2qp interaction and spurious state effects were considered in the present work and were omitted by SS.

Section II describes the theory behind the Coriolis decoupling model. The consequences of this model are described in detail, in Sec. III, for the nucleus ^{156}Er because this nucleus exhibits the essential features of decoupling and appreciable experimental data on its yrast bands are available.[14] The predictions of this model are similar for different regions of the periodic table, and thus Sec. IV gives a brief summary of the consequences when the model is applied to the nucleus ^{104}Pd. The general conclusions derived from this work are given in Sec. V.

II. THEORY

A. The Hamiltonian

The Hamiltonian describing the system of total angular momentum $\vec{I}$ which consists of two particles in orbits $\vec{j}_1$ and $\vec{j}_2$ coupled to an axially symmetric core rotating with angular momentum $\vec{R}$ can be written as[15]

$$H = H_0 + (\hbar^2/2\mathcal{I})\vec{R}^2 , \tag{1a}$$

$$\vec{R} = \vec{I} - \vec{J} , \tag{1b}$$

$$\vec{J} = \vec{j}_1 + \vec{j}_2 , \tag{1c}$$

$$H_0 = H_{s.p.}(1) + H_{s.p.}(2) + H_{int} , \tag{1d}$$

where $\vec{I}$, $\vec{R}$, $\vec{J}$, $\vec{j}_1$, and $\vec{j}_2$ are vector operators. $H_{s.p.}$ is the single particle Hamiltonian and H_{int} is the residual two-body Hamiltonian. The angular momentum coupling and the projections of the angular momenta on the different axes are defined in Fig. 1.

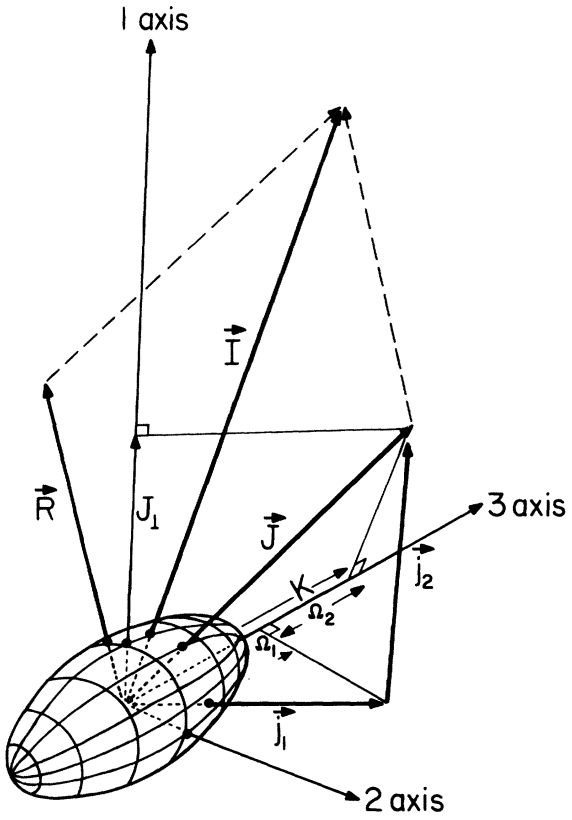

FIG. 1. Pictorial representation of the different spins, axes, and projections discussed in text.

B. Basis states

Strong coupling wave functions[15] were chosen as the basis states for the system, since the different parts of the Hamiltonian H have a simple form in this space; i.e.,

$$|IMK\Omega_1\Omega_2\rangle = \left(\frac{2I+1}{16\pi^2}\right)^{1/2}[D^I_{MK}(\chi^{\Omega_1}\chi^{\Omega_2})_A + R_\perp(D^I_{MK})R_\perp^{-1}(\chi^{\Omega_1}\chi^{\Omega_2})_A], \tag{2}$$

with the constraint that $K=\Omega_1+\Omega_2$ and $K\geq 0$. The D^I_{MK} are the usual rotation matrices,[15] and the χ^Ω are the solutions of $H_{s.p.}$ with the projection of j on the symmetry axis $\langle j_3\rangle=\Omega$ being a constant of motion. The second term in the bracket accounts for the axial symmetry where the operator $R_\perp$ corresponds to a 180° rotation about an axis in the 1-2 plane (see Fig. 1). The product wave function in the intrinsic frame $(\chi^{\Omega_1}\chi^{\Omega_2})_A$ is taken to be antisymmetric with respect to exchange of the two particles, i.e.,

$$(\chi^{\Omega_1}_\alpha\chi^{\Omega_2}_\beta)_A = \frac{1-P_{12}}{[2(1+\delta_{\alpha\beta}\delta_{-\Omega_1\Omega_2})]^{1/2}}\chi^{\Omega_1}_\alpha\chi^{\Omega_2}_\beta, \tag{3}$$

where P_{12} is the exchange operator.

If the single-particle wave function in the deformed well χ^Ω is expanded in terms of solutions for a spherical potential, i.e., χ^Ω_j, then the wave function becomes

$$|IMK\Omega_1\Omega_2\rangle = \left(\frac{2I+1}{16\pi^2}\right)^{1/2}\sum_{j_1j_2} C^{\Omega_1}_{j_1}C^{\Omega_2}_{j_2}[D^I_{MK}(\chi^{\Omega_1}_{j_1}\chi^{\Omega_2}_{j_2})_A + (-)^{I+j_1+j_2+2K}D^I_{M-K}(\chi^{-\Omega_1}_{j_1}\chi^{-\Omega_2}_{j_2})_A]. \tag{4}$$

C. $H_{\rm rot}$

The rotational part of the Hamiltonian can be written in the intrinsic frame of reference as

$$H_{\rm rot} = \frac{\hbar^2}{2\mathcal{I}}R^2 = \frac{\hbar^2}{2\mathcal{I}}\{[I(I+1)-K^2]-[\hat I_+\hat J_- + \hat I_-\hat J_+]+[(j_1^2-\Omega_1^2)+(j_2^2-\Omega_2^2)+(\hat j_{1+}\hat j_{2-}+\hat j_{1-}\hat j_{2+})]\}, \tag{5}$$

where the operators are $\hat I_\pm \equiv \hat I_x \pm i\hat I_y$ and $\hat J_\pm \equiv \hat J_x \pm i\hat J_y$. The quantity in the first bracket of Eq. (5) is easily recognized as the diagonal term giving rise to the normal $I(I+1)$ spacing for rotational bands based on two particles coupled with the projection of $\hat J$ on the symmetry axis (3 axis) equal to K. The second term is the particle-rotation coupling, or Coriolis term, while the last square bracket contains the two-particle analog of the so called "recoil" term, usually ignored in one-particle calculations. The evaluation of the matrix elements of $H_{\rm rot}$ is straightforward in this space by recalling that

$$\hat j_\pm|\chi^\Omega_j\rangle = [(j\mp\Omega)(j\pm\Omega+1)]^{1/2}|\chi^{\Omega\pm1}_j\rangle, \tag{6a}$$

$$\hat I_\pm|D^I_{MK}\rangle = [(I\pm K)(I\mp K+1)]^{1/2}|D^I_{MK\mp1}\rangle. \tag{6b}$$

D. $H_{\rm s.p.}$

The Nilsson model was chosen to describe $H_{s.p.}$. The single-particle eigenvalues and eigenfunctions for the model were taken from the calculations of Chi.[16] The oscillator constant was taken to be $\hbar\omega = 41/A^{1/3}$ MeV and the spin-orbit parameter $K=0.05$. The parameter μ for the $\vec l\cdot\vec l$ term was taken equal to 0.625 and 0.630 for the $N=4$ and 5 proton oscillator shells, respectively, and 0.450, 0.450, and 0.448 for the $N=4$, 5, and 6 neutron oscillator shells, respectively.

E. Quasiparticle transformation

The residual nucleon-nucleon interaction manifests itself not only in the interaction between the two valence nucleons $H_{\rm int}$, which is included explicitly in the Hamiltonian [Eq. (1)], but also in the interaction between the valence nucleons and the nucleons in the core. This latter effect was taken into account by assuming the pairing interaction and using the simplest elements of the BCS approximation,[17] i.e., by making the usual transformation to quasiparticles.

This transformation is straightforward for one-body operators. The matrix elements of $\vec j_1^{\,2}$ and $\vec j_2^{\,2}$, however, have nonzero two-body parts after the quasiparticle transformation. Fortunately, these operators only occur in the recoil term of the Hamiltonian, which is significantly smaller than the rotation particle coupling term for high-spin states. Therefore, the matrix elements of $\vec j_1^{\,2}$ and $\vec j_2^{\,2}$ were evaluated assuming they were one-body operators. It can be shown that this approximation introduces less than a 20% uncertainty in these matrix elements.

F. Residual two-quasiparticle interaction H_{int}

The residual interaction between the two quasiparticles is the most complex part of the Hamiltonian to evaluate. Fortunately, the Coriolis matrix elements can be an order of magnitude larger than the matrix elements of the residual two-quasiparticle interaction H_{int} for the high-spin states of interest in the present work. Therefore calculations were performed using two schematic forms for H_{int}.

The first approximation, approximation A, assumed that the residual two-quasiparticle interaction H_{int} was diagonal, with matrix elements equal to 200 keV and with the signs given by the Gallagher rule.[18] This was the most extreme and simplest approximation which schematically included the most significant part of the residual interaction, that is, the splitting of the $K=|\Omega_1 \pm \Omega_2|$ doublets. Most of the calculations were performed using this simple approximation.

The second approximation, approximation B, assumed the residual two-quasiparticle interaction to be a surface δ interaction[19] (SDI) of the form

$$H_{\text{SDI}} = -4\pi G \delta(\Omega_{ij}) \delta(r_i - R) \delta(r_j - R) . \tag{7}$$

This more realistic interaction was used to investigate the role of the two-body interaction in determining the observed rotational band behavior. The matrix elements of the residual interaction are given by

$$\langle IMK\alpha\beta 1 | H_{\text{SDI}} | IMK\gamma\delta 1\rangle$$

$$= -\frac{G}{2} \sum_J \{[(U_\alpha U_\gamma + V_\alpha V_\gamma)(U_\beta U_\delta + V_\beta V_\delta) + (-)^{\pi+J}(U_\beta U_\gamma + V_\beta V_\gamma)(U_\delta U_\chi + V_\alpha V_\delta)] F(\alpha\beta JK) F(\gamma\delta JK)$$

$$- (U_\alpha V_\beta - V_\alpha U_\beta)(U_\gamma V_\delta - V_\gamma U_\delta) G(\alpha\beta JK) G(\gamma\delta JK)\} , \tag{8}$$

where

$$F(\alpha\beta JK') \equiv \sum_{ab} C_a^\alpha C_b^\beta (a\alpha b\beta | JK')(a\tfrac{1}{2} b - \tfrac{1}{2} | J0) \left[\frac{(2a+1)(2b+1)}{(2J+1)(1+\delta_{ab}\delta_{\alpha-\beta})}\right]^{1/2} (-)^{l_\alpha + b + 1/2} ,$$

$$G(\alpha\beta JK') \equiv \sum_{ab} C_a^\alpha C_b^\beta (a\alpha b\beta | JK')(a\tfrac{1}{2} b\tfrac{1}{2} | J1) \left[\frac{(2a+1)(2b+1)}{(2J+1)(1+\delta_{ab}\delta_{\alpha-\beta})}\right]^{1/2} ,$$

and where the quantum numbers a and α designate j and Ω, respectively. The U_α and V_α are the usual occupation probabilities. The pairing factors in the second term of Eq. (8) are generally small and thus this term is negligible. Therefore the calculations were all performed neglecting this second term. Note that the pairing factor in the first term is also small if $\pi + J$ is odd. Since we are dealing with identical nucleons in the present work, any spin exchange term in the residual interaction can be absorbed into the strength of the interaction G.

The difference in the results of calculations using approximations A and B is discussed in Sec. III.

G. Spurious state problem

The evaluation and diagonalization of the Hamiltonian in the chosen basis is relatively straightforward for the negative-parity states. However, the calculation for the positive-parity states is unreliable due to the admixture of the spurious seniority zero state for $K=0^+$ two-quasiparticle bands.[20] Diagonalization of the pairing force showed that due to the presence of this spurious state about 30% of the Corioulis strength was redistributed among the states of interest. Therefore all matrix elements involving the mixing between $K=0$ and other states were attenuated by 30% to schematically account for this effect.

H. Transformation to the $|IMRj_1j_2J\rangle$

An understanding of the decoupling mechanism is much facilitated by transforming the wave function $|IM\rangle$ into a basis where R and J are good quantum numbers using the relation

$$\langle IMRj_1j_2J | IM\rangle = \tfrac{1}{2} \sum_{\substack{K>0 \\ \Omega_1\Omega_2}} A^{IM}_{K\Omega_1\Omega_2} C^{\Omega_1}_{j_1} C^{\Omega_2}_{j_2} (-)^{J-K} (IKJ-K | R0)(j_1\Omega_1 j_2\Omega_2 | JK)[1+(-)^R] , \tag{9}$$

where $A^{IM}_{K\Omega_1\Omega_2}$ are the expansion coefficients in the $|IMK\Omega_1\Omega_2\rangle$ basis, that is,

$$|IM\rangle = \sum_{\substack{K>0 \\ \Omega_1\Omega_2}} A^{IM}_{K\Omega_1\Omega_2} |IMK\Omega_1\Omega_2\rangle . \tag{10}$$

Note that for axial symmetry only even values of R occur. The R distributions now can be obtained by summation of the squares of the overlap [Eq. (9)] over all possible $j_1 j_2 J$, and similarly, the J distributions were obtained by summation over $j_1 j_2$ and R. The results of this procedure are discussed in Sec. 3.

I. Coriolis antipairing

The increase in the moment of inertia and reduction in the pairing gap with increasing spin are two major consequences of Coriolis antipairing. The former effect was schematically included in the present calculations by assuming that the moment of inertia was a function of the rotation of the core (R) and by expressing the eigenfunctions in the $|IMRj_1j_2J\rangle$ basis, i.e., where R is a good quantum number. The excitation energies $E_X(I)$ for the zero-quasiparticle band, i.e., the ground state band below the backbend, directly determines this variable moment of inertia since $R=I$ for this band, i.e.,

$$\frac{2\mathcal{I}(R)}{\hbar^2} = \frac{I(I+1)}{E_X(I)} . \tag{11}$$

For simplicity the variation of $2\mathcal{I}(R)/\hbar^2$ was chosen to be linear in R since no attempt was made to fit exactly the experimental energies in the present work. This linear assumption is only approximately true for the ground state band, and it introduces some discrepancies in the calculated energies of the zero-quasiparticle states and presumably comparable discrepancies in the calculated two-quasiparticle energies.

It is important to note that the moment of inertia given by Eq. (11) is not the same as the instantaneous value defined in conventional backbending diagrams but is the average of the instantaneous values up to spin I.

J. Measure of decoupling

A measure of the amount of decoupling is required in order to make a quantitative interpretation of the eigenvectors. Analogy with the classical situation would suggest that the average projection of the intrinsic spin $\vec{J}$ onto the rotation axis $\vec{R}$, i.e., J_R defined as

$$J_R = \left\langle \frac{\vec{J}\cdot\vec{R}}{|\vec{R}|} \right\rangle \tag{12}$$

is an appropriate measure. This is certainly true for $R \gg J$. However, for small R the direction and magnitude of $\vec{R}$ varies widely and thus J_R is not too useful a definition. Also, all $\langle J_R\rangle$ must be negative for $I < (\langle J^2\rangle + \langle R^2\rangle)^{1/2}$ and become positive for maximum alignment as $I \to \infty$. Inspection of the Hamiltonian shows that the alignment of $\vec{J}$ with $\vec{I}$ is a more appropriate measure. That is, the projection of $\vec{J}$ onto $\vec{I}$ given by

$$J_I = \frac{\langle \vec{J}\cdot\vec{I}\rangle}{I(I+1)} . \tag{13}$$

Of course, $J_I \simeq J_R$ for $I \to \infty$. The difficulty with this definition is that even in the strong coupling limit, where the rotation-particle coupling term $(\hat{I}_+\hat{J}_- + \hat{I}_-\hat{J}_+)$ is zero, $\vec{I}\cdot\vec{J} = K^2$, which can be large for large K. The contribution of K to the alignment J_I can be eliminated by calculating the expectation value of the projection of $\vec{J}$ onto the component of $\vec{I}$ perpendicular to the symmetry axis, i.e., $J_\perp$ given by

$$\begin{aligned} J_\perp &= \left\langle \frac{\vec{I}\cdot\vec{J} - K^2}{|\vec{I} - \vec{I}|_3} \right\rangle , \\ J_\perp &= \left\langle \frac{\hat{I}_+\hat{J}_- + \hat{I}_-\hat{J}_+}{[I(I+1) - K^2]^{1/2}} \right\rangle . \end{aligned} \tag{14}$$

The projection $J_\perp$ (illustrated in Fig. 1) is just the renormalized rotation-particle coupling term of Eq. (5), and is zero in the strong coupling limit for $K \neq \frac{1}{2}$ bands. Equation (5) can be rewritten in terms of $J_\perp$ as

$$\langle H_{\text{rot}}\rangle \approx (\hbar^2/2\mathcal{I}) \Big\{ I(I+1) - 2J_\perp [I(I+1)]^{1/2} + \langle J^2 - 2K^2\rangle + \frac{\langle K^2\rangle J_\perp}{[I(I+1)]^{1/2}} \Big\} \tag{15}$$

for $I \gg K$.

It is now possible to compare this to the classical picture of a rotor with angular momentum R and a decoupled particle with angular momentum C which is aligned with R, i.e., $I = R + C$. The spectrum is then given by

$$\begin{aligned} \langle H_{\text{decoupled}}\rangle &= (\hbar^2/2\mathcal{I})R(R+1) \\ &= (\hbar^2/2\mathcal{I})[I(I+1) - 2CI + C(C-1)] . \end{aligned} \tag{16}$$

One can immediately recognize the similarity between Eqs. (15) and (16) with $J_\perp[I(I+1)/I^2]^{1/2} \approx C$, providing that the last term in Eq. (15) is small or nearly constant. This is satisfied best for large I. Thus, $J_\perp$ is an excellent measure of decoupling since the degree to which it is constant measures the degree of decoupling and its value gives, for large I, the effective aligned spin of the

uncoupled particles.

The degree of decoupling of the individual quasiparticles can be also determined separately by defining

$$j_\perp = \left\langle \frac{\vec{j}\cdot\vec{I} - \Omega K}{[I(I+1) - K^2]^{1/2}} \right\rangle . \tag{17}$$

This is only relevant for negative-parity states, where the two particles are distinguishable.

The interpretation of the value of $J_\perp$ for the coupled two-quasiparticle states and the values of $j_\perp^{(+)}$ and $j_\perp^{(-)}$ for the individual quasiparticles are discussed in Sec. III.

K. Mixing of the zero- and two-quasiparticle bands

The interaction between the 0qp ground band and the 2qp bands was not included in the present calculation because experimental and theoretical evidence suggests that the interband interaction matrix elements are very small.

Experimentally the intersecting bands have been observed both above and below the intersection in two nuclei,[21,22] ^{154}Gd and ^{156}Dy. The observed γ branching implies ratios of the interband to intraband $B(E2)$'s of 10^{-3} for states away from the intersection. Assuming a two-band mixing model and similar intrinsic quadrupole moments in both bands and using the observed γ branching and level energies leads to interaction matrix elements between the bands of about $\lesssim$25 keV at spin 16^+. Forking seen[10,23] in ^{126}Ba and ^{190}Pt implies similar small matrix elements at the band intersection. These interband interaction matrix elements are considerably smaller than the level spacings and thus will perturb the bands only near the intersection.

Interaction matrix elements of about 25 keV between the 16^+ states of the interacting bands are about two orders of magnitude smaller than typical Coriolis matrix elements. This behavior can be understood by considering many identical particles in a multiconfiguration space under the influence of a Hamiltonian with pairing, rotational, and deformed single-particle parts. The pairing and rotational Hamiltonians are quasispin scalars since a multipole expansion of these Hamiltonians has only odd-rank terms. Since these quasispin scalars conserve seniority, only the quadrupole deformed field remains to mix states of different seniority. The present two-quasiparticle-plus-rotor model calculations show the yrast decoupled two $i_{13/2}$ quasineutron eigenfunctions become increasingly localized aroung $J=12$ and $R=I-12$ with increasing spin I. On the other hand, the zero-quasiparticle ground band has $I=R$ for a fully paired state. The quadrupole ($\lambda=2$) deformed field can mix these bands, which have very different rotational frequencies, only by a high-order process, hence the interaction will be weak. An equivalent statement is that the Coriolis force does not couple states with differing R and thus the two bands interact only via the overlap with weak components of the wave functions. This overlap becomes progressively smaller with increasing spin I due to the increased localization in R space of the decoupled states. The present calculations suggest an interband interaction strength of $\lesssim$100 keV at the intersection. However, this calculated interaction strength may be rather sensitive to the approximations made.

We can therefore conclude that, within this model, mixing between zero- and the aligned two-quasiparticle bands can be ignored.

L. Parameters of the calculation

It is important to consider the influence of the adjustable parameters on the results of the calculation.

The moment of inertia parameter $\hbar^2/2\mathcal{I}$ essentially scales the excitation energies without changing the qualitative appearance of the spectrum or wave functions. A doubling of $\hbar^2/2\mathcal{I}$ changed the wave functions by $\lesssim$2%. The other adjustable parameter in the calculation is the pairing gap Δ. Since H_R is much larger than variations in $H_{s.p.}$, then the primary influence of a change in Δ is to shift the whole two-quasiparticle spectrum by twice this change in energy provided Δ remains larger than typical single-particle energy separations. Small changes in the deformation parameter β produce only minor effects through changes in single-particle energies and an energy scaling through changes in Coriolis matrix elements. It is concluded that reasonable variations in the parameters produces small differences in the qualitative appearance of the 2qp spectrum and the calculated wave functions. This suggests that a qualitative reproduction of the observed phenomena will reflect more the consequences of the physics contained in the model rather than a fortuitious choice of parameters.

A quantitative fit to the experimental energies requires the choice of a proper scale, by appropriate choice of the moment of inertia, while the absolute energies are obtained by appropriate choice of Δ. Table I shows the sets of parameters used in the calculations. The column marked β gives the nuclear deformation derived from the known $B(E2; 0^+ \rightarrow 2^+)$ values. The linear variation coefficients a and b of the dependence of $2\mathcal{I}/\hbar^2$ on $\langle R \rangle$ are given in the following four columns. These are obtained by fitting to the known ground band

TABLE I. Parameters used in the calculations.

		$\frac{2\mathcal{J}}{\hbar^2}=a+b\langle R\rangle$												
		0qp		2qp							Nilsson orbitals			
Nucleus	β	a	b	a	b	Type	λ ($\hbar\omega$)	Δ_{calc} (MeV)	Δ_{eff} (MeV)	Orbital parity	quasiparticle energies (MeV)			
$^{156}_{68}Er_{88}$	+0.26	20	2	20	2	$2q\nu$	5.85	1.00	0.70	+	$\frac{1}{2}$[660]	$\frac{3}{2}$[651]	$\frac{5}{2}$[642]	$\frac{7}{2}$[633]
											1.137	1.000	1.339	2.307
										−	$\frac{1}{2}$[530]	$\frac{1}{2}$[541]	$\frac{3}{2}$[532]	
											1.271	2.232	1.137	
						$2q\pi$	5.28	1.00	0.70	−	$\frac{1}{2}$[541]	$\frac{5}{2}$[532]	$\frac{7}{2}$[523]	$\frac{9}{2}$[514]
											1.413	1.622	1.000	1.870
										+	$\frac{1}{2}$[411]	$\frac{3}{2}$[411]	$\frac{5}{2}$[413]	$\frac{7}{2}$[404]
											1.175	1.099	1.313	1.578
$^{104}_{46}Pd_{58}$	+0.21	8	2	15	0.9	$2q\nu$	5.25	1.30	0.85	−	$\frac{1}{2}$[550]	$\frac{3}{2}$[541]		
											1.302	1.430		
										+	$\frac{1}{2}$[420]	$\frac{3}{2}$[422]	$\frac{5}{2}$[413]	$\frac{1}{2}$[431]
											1.831	1.703	1.461	2.938
						$2q\pi$	4.60	1.50	1.05	+	$\frac{1}{2}$[440]	$\frac{3}{2}$[431]	$\frac{5}{2}$[422]	$\frac{7}{2}$[413]
											2.185	1.797	1.500	2.033
										−	$\frac{1}{2}$[301]			
											1.796			

energies in ^{156}Er. However, for ^{104}Pd it was assumed that the 2qp band had a more rigid rotational structure, i.e., smaller slope and larger intercept, than the 0qp band to reflect the fact that ^{104}Pd appears soft to deformation in its ground band. The presence of two quasiparticles could introduce more rigidity to the nuclear deformation. The column marked "type" indicates whether the calculation is for two quasiprotons ($2q\pi$) or two quasineutrons ($2q\nu$). The following column gives the Fermi level λ in units of $\hbar\omega$. The next column gives the values of the pairing gap Δ_{calc} taken from systematics.[24] These are the values used to calculate eigenvalues and eigenfunctions. The calculated spectrum was then shifted for better absolute agreement, resulting in effective pairing gap Δ_{eff} shown in the following column. This procedure was not iterated because it introduced negligible errors in eigenfunctions and ≤ 50 keV uncertainties in the calculated energies of the high-spin states. The orbitals and associated quasiparticle energies used in the calculation are given in the last part of Table I.

It must be emphasized that the above sets of parameters are not unique but they are typical of parameters used in other types of calculation for similar mass nuclei. They serve to demonstrate that quantitative fits indeed are not only possible but are not very difficult to obtain within this model.

III. APPLICATION TO ^{156}Er

A. Eigenvalues for ^{156}Er

The energy level spectrum of the two quasineutron yrast states in ^{156}Er, calculated using the variable moment of inertia given in Table I, is compared in Fig. 2 with the experimental data of Sunyar *et al.*[14] The eigenvalues and properties of the eigenvectors of the two-quasineutron states listed in Tables II and III were evaluated for a constant moment of inertia parameter $\hbar^2/2\mathcal{I} = 43.5$ keV, which corresponds approximately to the ground state moment of inertia for ^{156}Er. This constant moment of inertia produces eigenvalues twice as large as the variable moment of inertia for states with $I \approx 24$ and a change of less than 2% in the eigenvectors.

The calculations show that the positive-parity two-quasineutron band crosses below the zero-quasiparticle ground state band between the 10^+ and 12^+ states. The agreement between experiment and theory for the even-spin positive-parity states is remarkably good. The experimental odd-spin negative-parity states from 11^- to 23^- are also well reproduced by the theory. The calculated energies of the 9^- and 7^- states are appreciably higher than experiment. This disagreement is not surprising since the collective octupole correlations have been omitted and these should be important for the low-spin states where the residual

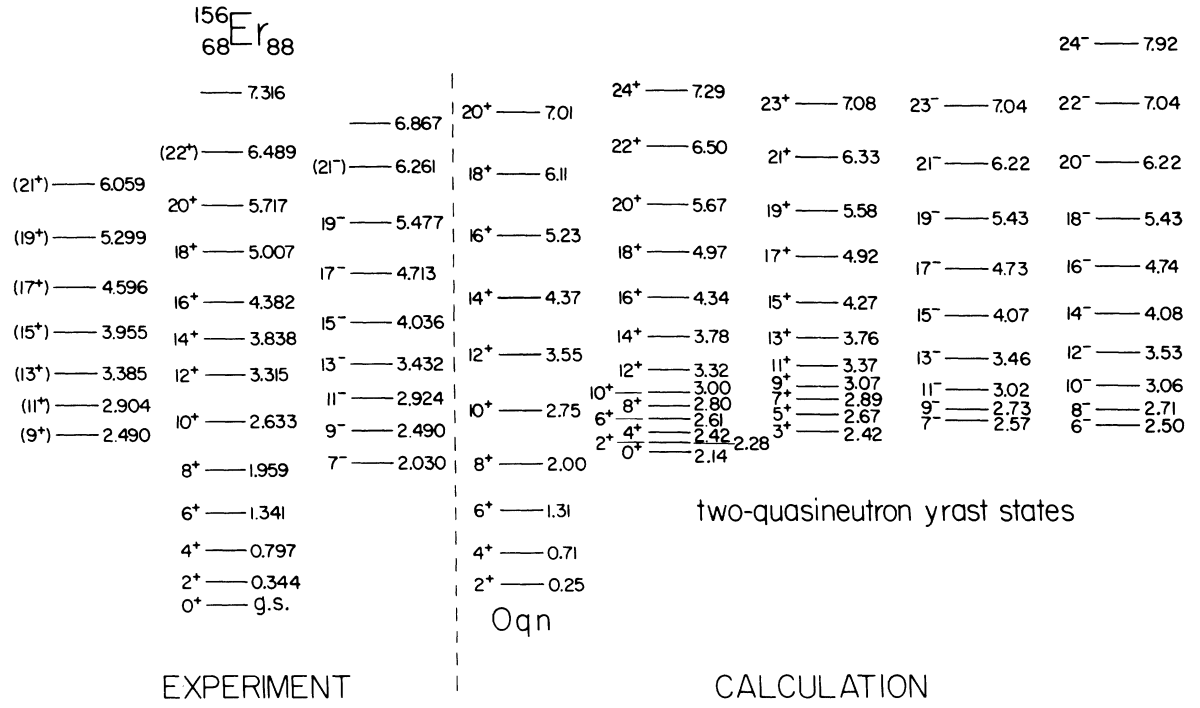

FIG. 2. Comparison of the calculated yrast two-quasineutron spectrum of ^{156}Er with experiment.

TABLE II. Properties of the two-quasineutron yrast states in ^{156}Er. Positive parity.

I^π	E_x	$\langle R \rangle$	$\langle J \rangle$	J_R	$J_\perp$	$\langle K \rangle$	$\lvert\langle I^\pi \rvert 23^+\rangle\rvert^2$	$\lvert\langle I^\pi \rvert 24^+\rangle\rvert^2$
0^+	2.769	1.91	1.91	−2.23	···	0	0.00	0.00
2^+	2.911	2.33	2.94	−2.17	1.43	0.77	0.00	0.00
4^+	3.098	2.76	4.37	−2.06	3.02	1.29	0.01	0.00
3^+	3.134	3.42	3.89	−2.72	1.53	1.85	0.00	0.00
6^+	3.321	2.96	6.17	−2.14	4.91	1.74	0.11	0.10
5^+	3.438	3.94	5.34	−2.90	3.37	2.21	0.04	0.03
8^+	3.524	3.08	8.37	−2.93	7.15	2.16	0.51	0.51
1^+	3.658	4.42	4.43	−4.66	0	1.00	0.00	0.00
7^+	3.715	4.24	7.26	−3.29	5.49	2.71	0.33	0.25
10^+	3.730	2.98	9.78	−1.66	8.57	2.34	0.80	0.85
9^+	3.957	4.40	9.12	−3.43	7.51	3.00	0.77	0.63
12^+	4.153	3.44	10.25	3.49	9.01	2.37	0.88	0.95
11^+	4.328	4.82	9.88	−0.65	8.28	3.05	0.93	0.78
14^+	4.889	4.85	10.42	6.51	9.17	2.36	0.89	0.98
13^+	4.988	5.93	10.16	2.27	8.54	3.03	0.97	0.84
16^+	5.962	6.58	10.52	7.69	9.24	2.35	0.89	0.99
15^+	5.979	7.42	10.28	4.09	8.65	3.01	0.99	0.86
17^+	7.313	9.12	10.36	5.21	8.71	2.98	1.0	0.87
18^+	7.378	8.42	10.58	8.30	9.29	2.38	0.89	0.99
19^+	8.993	10.91	10.41	5.94	8.74	2.96	1.0	0.88
20^+	9.139	10.32	10.62	8.67	9.31	2.32	0.88	1.0
21^+	11.020	12.78	10.45	6.46	8.76	2.96	1.0	0.88
22^+	11.248	12.25	10.65	8.91	9.33	2.31	0.88	1.0
23^+	13.395	14.65	10.46	6.82	8.78	2.96	≡1	0.88
24^+	13.703	14.18	10.65	9.08	9.34	2.29	0.88	≡1

TABLE III. Properties of the two-quasineutron yrast states in ^{156}Er. Negative parity.

I^π	E_x	$\langle R \rangle$	$\langle J \rangle$	J_R	$J_\perp$	$j_\perp^{(+)}$	$\langle K \rangle$	$\lvert\langle I^\pi \rvert 23^-\rangle\rvert^2$	$\lvert\langle I^\pi \rvert 24^-\rangle\rvert^2$
6^-	3.272	3.47	6.98	−3.65	5.91	5.27	1.58	0.01	0.06
5^-	3.347	3.70	6.31	−3.83	4.99	5.44	1.66	0.07	0.03
4^-	3.354	3.73	6.57	−5.32	4.92	5.42	1.71	0.00	0.04
7^-	3.358	3.71	8.43	−5.71	7.49	5.40	1.88	0.84	0.15
2^-	3.393	2.90	4.03	−3.40	2.86	5.24	0.74	0.03	0.03
3^-	3.400	3.13	4.90	−3.76	3.74	4.99	1.36	0.03	0.03
9^-	3.442	3.15	8.85	−2.30	8.10	5.46	1.65	0.94	0.12
8^-	3.501	3.78	7.37	−1.30	6.31	5.40	1.64	0.03	0.30
1^-	3.675	3.81	4.20	−4.37	1.76	1.87	0.88	0.00	0.02
0^-	3.715	3.76	3.76	−3.76	···	···	0.0	0.06	0.01
11^-	3.824	3.68	9.01	2.84	8.31	5.49	1.53	0.97	0.10
10^-	3.925	4.05	8.20	1.05	7.38	5.58	1.57	0.09	0.93
13^-	4.534	5.13	9.10	5.52	8.40	5.51	1.46	0.99	0.09
12^-	4.614	5.29	8.30	3.86	7.54	5.60	1.45	0.08	0.96
15^-	5.582	6.85	9.12	6.59	8.45	5.52	1.41	1.00	0.08
14^-	5.634	6.94	8.32	5.27	7.59	5.61	1.40	0.08	0.97
17^-	6.974	8.69	9.14	7.16	8.48	5.53	1.38	1.00	0.07
16^-	7.007	8.76	8.34	5.96	7.62	5.61	1.36	0.07	0.98
19^-	8.711	10.59	9.17	7.52	8.50	5.53	1.35	1.00	0.07
18^-	8.719	10.66	8.36	6.38	7.64	5.62	1.34	0.07	0.98
20^-	10.779	12.56	8.36	6.64	7.65	5.62	1.31	0.07	0.98
21^-	10.794	12.51	9.18	7.75	8.52	5.54	1.33	1.00	0.06
22^-	13.185	14.49	8.37	6.83	7.66	5.63	1.30	0.07	0.99
23^-	13.224	14.46	9.19	7.92	8.53	5.54	1.32	≡1	0.06
24^-	15.938	16.45	8.37	6.97	7.67	5.63	1.28	0.06	≡1

two-quasiparticle interaction is comparable in strength to the Coriolis interaction. The calculated 5^-, 3^-, and 1^- states, not shown in Fig. 2, are almost degenerate with or lie above the calculated 7^- state and have a small wave function overlap with the higher odd-spin negative-parity states.

The location of the unnatural-parity states is a stringent test of this model. The even-spin negative parity states are predicted to have a characteristic decoupled band structure. That is, the I^-_{odd} and $I^-_{\text{odd}} - 1$ states are almost degenerate. The same situation occurs for the positive-parity states where the I^+_{even} and $I^+_{\text{even}} - 1$ states are close in energy.

The results of the proton calculation indicate that the two-quasiproton states lie considerably higher in excitation energy than the neutron states. The energy differences for the even-spin positive-parity states vary from over 500 keV for the 6^+ to over 2.1 MeV for the 24^+ states. For the odd-spin negative-parity states, the differences vary from 320 keV for the 7^- to over 2 MeV for the 23^- states, while for the even-spin negative-parity states they vary from 180 keV for the 8^- to over 1.6 MeV for the 24^- states. Except in the case of the states in the vicinity of the onset of decoupling, these differences are considerably larger than the typical matrix elements of the residual two-body interaction, demonstrating that mixing between the proton and neutron states is unlikely. Since we find that the yrast states are neutron states, the following discussion will be confined only to the neutron states.

B. Eigenvectors for ^{156}Er

The eigenvectors have been transformed into the $|IMRj_1j_2J\rangle$ basis with the aid of Eq. (9) in order to investigate their decoupled structure. The J and R distributions were calculated for the yrast states and these are plotted in Figs. 3 and 4, respectively. The R distribution is plotted as the difference $R - I$

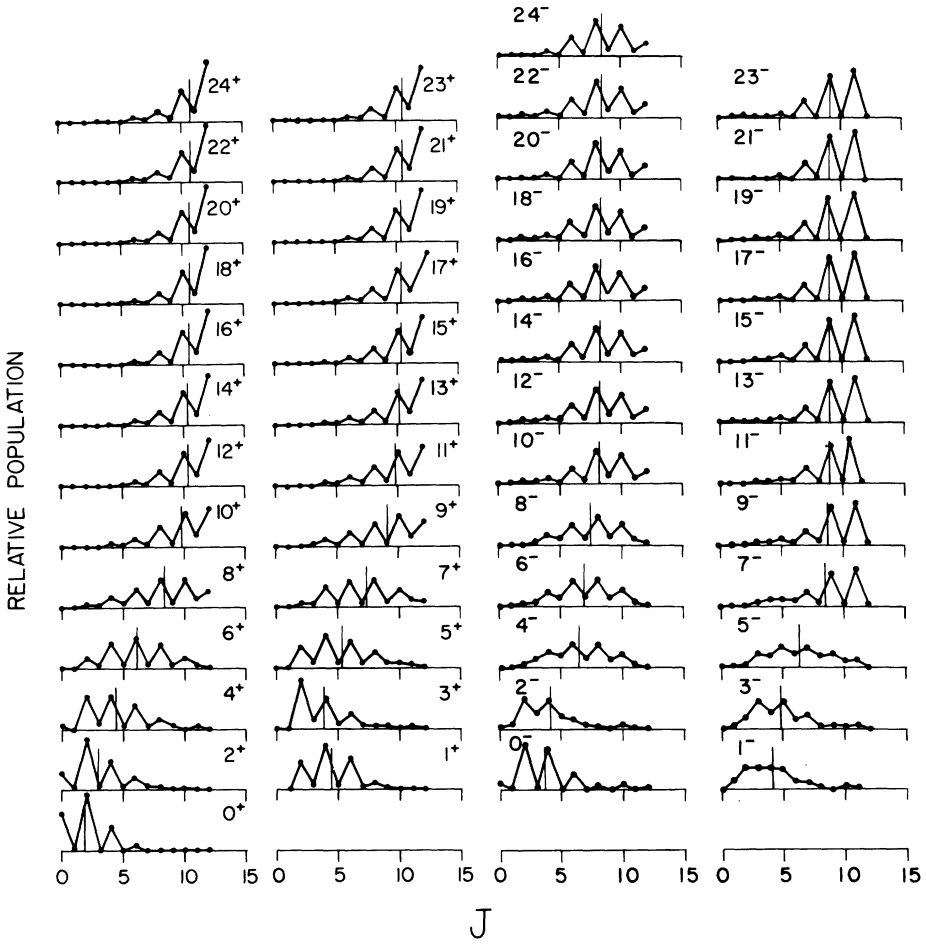

FIG. 3. Relative populations of the J substates for the two-quasineutron yrast states in ^{156}Er. The thin vertical lines indicate mean values $\langle J \rangle$.

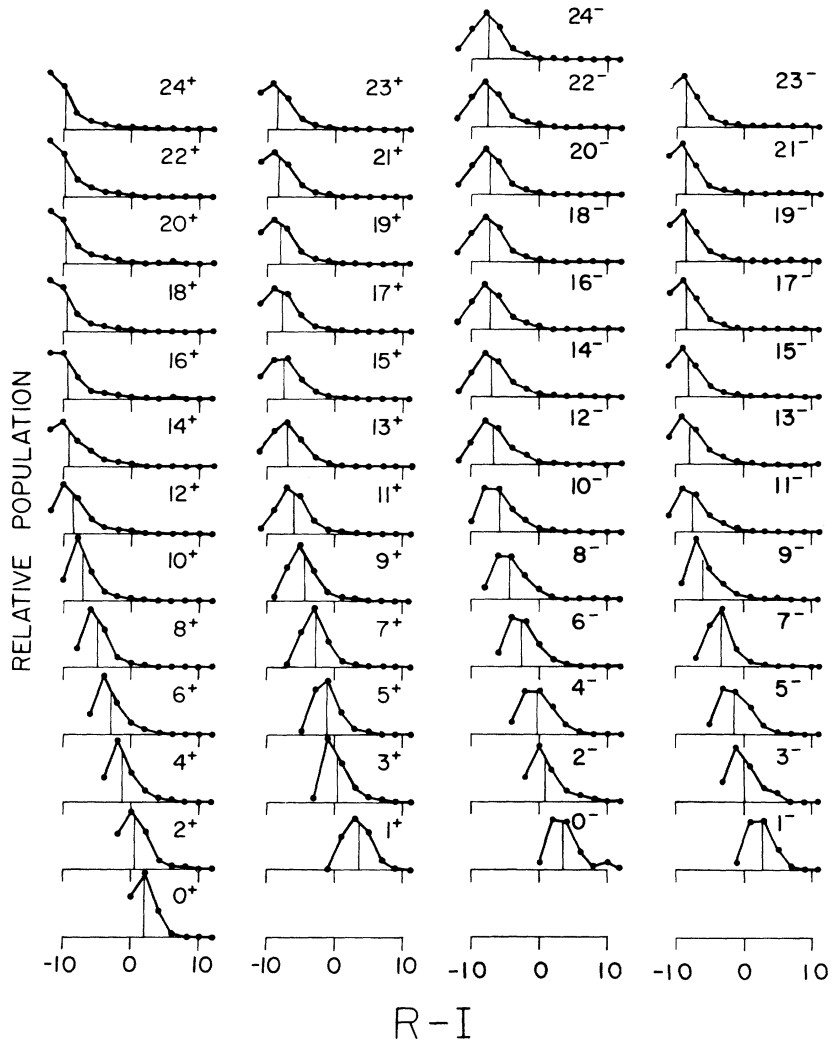

FIG. 4. Relative populations of the R substates for the two-quasineutron yrast states in ^{156}Er. The thin vertical lines indicate mean values $\langle R \rangle$.

in order to facilitate visual observation of the changes in the distributions for different values of I. The eigenvectors were also used to evaluate the expectation values of the magnitudes of $\vec{J}$, $\vec{R}$, J_R, $J_\perp$, K, $j_\perp^{(+)}$, and $j_\perp^{(-)}$ for the two-quasineutron states. The operators J_R, $J_\perp$, $j_\perp^{(+)}$ (and $j_\perp^{(-)}$) are defined by Eq. 12, 14, and 17, respectively. The values of $\langle R \rangle$, $\langle J \rangle$, J_R, $J_\perp$, and $\langle K \rangle$ are listed in Table II for the positive-parity yrast two-quasineutron states and in Table III for the negative-parity yrast two-quasineutron states. In addition, the values of $j_\perp^{(+)}$ are given for the negative-parity states in Table III. The last two columns in Tables II and III give the squares of the overlaps of the intrinsic wave function of each yrast two-quasineutron state with those of the same parity $I=23$ and $I=24$ yrast states, respectively.

Inspection of the J and $R-I$ distributions shown in Figs. 3 and 4 reveals that for $I \geq 12$ the yrast spectrum separates into four distinct bands; the even-spin positive-parity, odd-spin positive-parity, even-spin negative-parity, and odd-spin negative-parity, each with its own characteristic J and $R-I$ distribution.

It is easy to understand the remarkable odd-even J staggering in the J distributions shown in Fig. 3. One must keep in mind that, according to the decoupling picture, the yrast states are those that have the maximum $|\vec{J}|$, and where this $\vec{J}$ is maximally aligned with $\vec{R}$. But for such full alignment, one has

$$|\vec{I}| = |\vec{R}| + |\vec{J}| . \tag{18}$$

Since R is always even, for axial symmetry, only odd J can contribute to odd I and even J to even I, for fully aligned states. This has somewhat

different consequences for the positive- and negative-parity states.

The wave functions of the positive-parity states are obviously dominated by the $(i_{13/2})^2$ configurations. The spins of two neutrons in the same orbital can couple only to even J (due to the Pauli exclusion principle). Therefore, mostly even-J values contribute to both even- and odd-I states of positive parity. This is in conflict with the previous argument where only odd J are allowed for full alignment for odd-I positive-parity states. Thus one can say that the calculated odd-spin positive-parity states are not fully aligned. This, in turn, means that these states need relatively more rotation, i.e., excitation energy, for a particular total spin, than their even I counterparts, causing the odd-even splitting in the spectrum of the positive-parity yrast states.

The situation for the negative-parity states is a little more subtle. Since the two nucleons are distinguishable here (they have opposite parities), the Pauli exclusion principle allows both odd- and even-J states and thus full alignment of J with the rotation can occur for both odd- and even-I states. However, in the space of the Nilsson orbits considered in this calculation, the maximum allowable intrinsic spin, with appreciable probability, is $(h_{9/2}i_{13/2})$ coupled to $J=11^-$. Since this J value is odd, it can contribute only to the odd-I states for full alignment. The maximum J value allowed for the fully aligned even-I states is 10^-. Supposing the negative-parity yrast states contain mostly their maximum J values, then the odd-spin states of spin I will have the same R (and thus the same excitation energy), as the even-spin states of spin $I-1$ [see Eq. (18)], if they are both fully aligned. This degeneracy is clearly borne out out in the spectrum in Fig. 2.

It must be pointed out, however, that these calculations were restricted to only a few single-particle orbitals due to limited computer size. Although the truncation was selected to minimize the errors for the states of interest, this calculation is inadequate for very high-spin states, where complete $N=5$ or $N=6$ major shells should be included. The increasing significance of the $(h_{11/2}i_{13/2})^{J=12^-}$ configuration in such case would eventually cause a reversal in the odd-even splitting of the negative parity yrast states.

Further insight into the alignment behavior is gained by studying the expectation values $\langle R\rangle$, $\langle J\rangle$, and $J_\perp$ plotted for the yrast, yrast+1, and yrast+2 bands, shown in Figs. 5, 6, and 7, respectively. The rotational energy equals $(\hbar^2/2\mathcal{I})R(R+1)$ and thus the plot of $\langle R\rangle$ (Fig. 5) illustrates all the features shown by the energy level spectrum. Both the energy spectrum and $\langle R\rangle$ exhibit an odd-even splitting, and for $I\geq 12$ the gradient $\Delta R/\Delta I$ approaches unity, i.e., $\Delta R\simeq 2$ for each band.

The rigidity in the J distribution for $I>12$ is illustrated by the plot of $\langle J\rangle$ given in Fig. 6. This same feature occurs for the (yrast+1) and (yrast+2) bands. The expected odd-even I staggering in the $\langle J\rangle$ plot is also borne out.

The clearest understanding of the alignment behavior comes from studying the values of $J_\perp$, the projection of $\vec{J}$ onto the component of $\vec{I}$ perpendicular to the symmetry axis, shown in Fig. 7, and J_R, the average projection of $\vec{J}$ onto $\vec{R}$. The magnitudes of $J_\perp$ achieve a limiting value for $I\geq 10$. These limiting values of $J_\perp$ appear to be "quantized" and the whole calculated two-quasiparticle spectrum can be divided into definite bands with each band having a distinct value of $J_\perp$. In addition, the magnitudes of $J_\perp$ correlate with the excitation energies, with the yrast bands having the largest positive values of $J_\perp$, and the antialigned bands with the highest excitation energy, having the most negative values of $J_\perp$, equal in magnitude to those of the yrast bands. The ex-

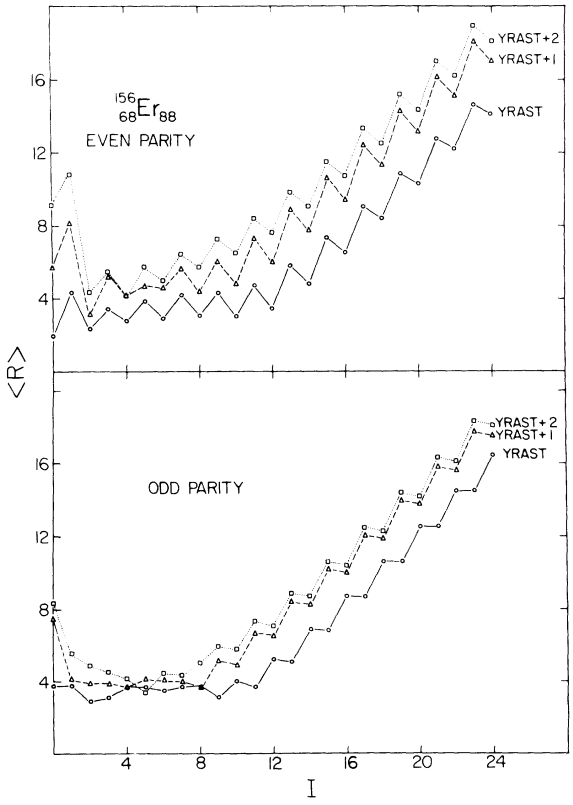

FIG. 5. Plot of $\langle R\rangle$, the average rotation of the core, versus I for some of the lowest two-quasineutron bands in ^{156}Er.

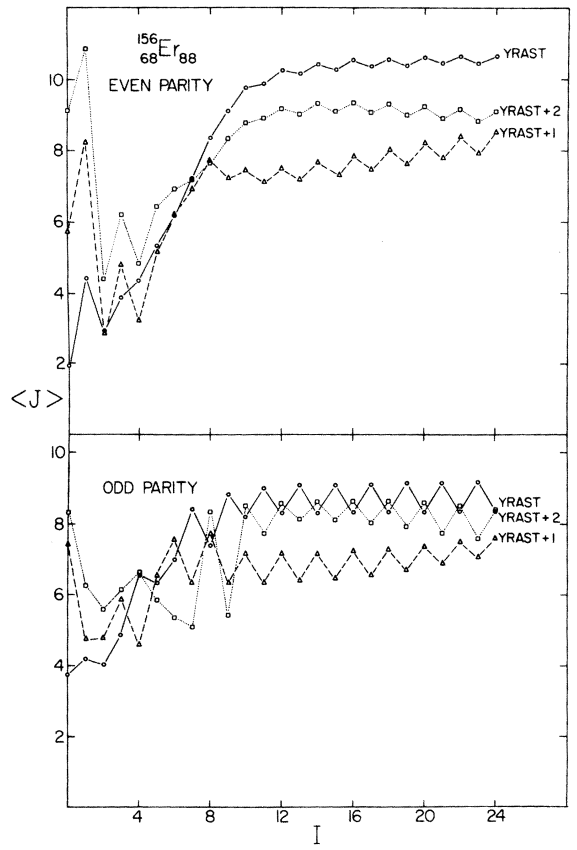

FIG. 6. Plot of $\langle J\rangle$, the average intrinsic spin, versus I for some of the lowest two-quasineutron bands in ^{156}Er.

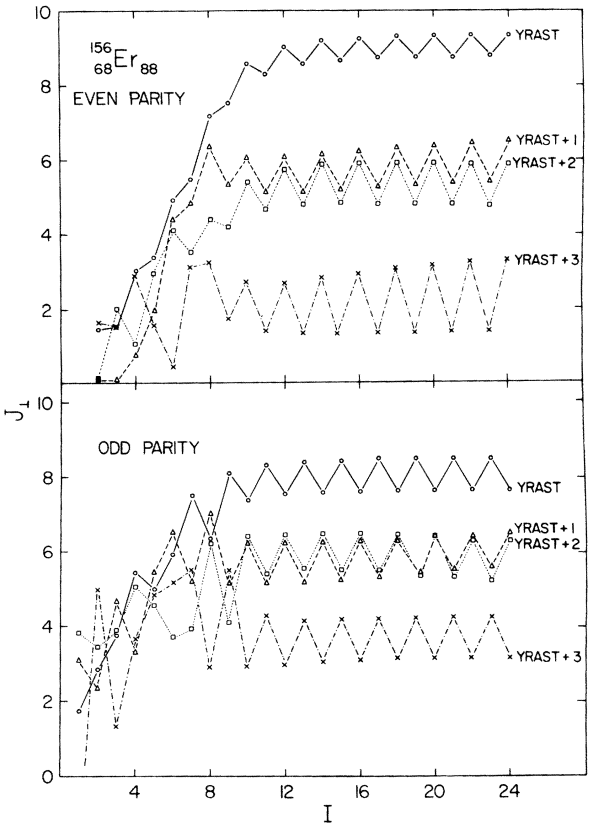

FIG. 7. Plot of $J_\perp$, the average projection of the intrinsic spin $\vec{J}$, on the component of $\vec{I}$ perpendicular to the symmetry axis for some of the lowest two-quasineutron bands in ^{156}Er.

pectation value $\langle J_R\rangle$ also exhibits characteristic behavior for each band but the values are more dependent on I, since they reach their limiting values much more slowly as discussed in Sec. II J. Figures 6 and 7 illustrate that $\langle J\rangle$ and $J_\perp$ become constants of motion for each band.

It is possible to estimate the spectrum of values of $J_\perp$ and hence the location in energy of the different bands by considering the limit of complete decoupling. Then the rotational part of the Hamiltonian can be approximated by Eq. (15). For large I the values of $\langle J\rangle$ and $J_\perp$ are constants of motion for the two dominant terms in the Hamiltonian, i.e., $(\hbar^2/2\mathcal{I})\{I(I+1)-2[I(I+1)]^{1/2}J_\perp\}$, and the band with lowest energy has the most positive value of $J_\perp$. The last two terms in the Hamiltonian [Eq. (15)] split the degeneracy for each $J_\perp$ the band with lowest $\langle J\rangle$ lying lowest in energy. For small $\langle K\rangle$ this splitting is proportional to $\langle J^2\rangle$. Thus, for each value of $J_\perp$ the most aligned state, i.e., $J_\perp \simeq J$, is lowest in energy, the $J=J_\perp+1$ band is next lowest, etc. The calculations show this to be generally correct, although each state is a mixture of several $|JJ_\perp\rangle$ configurations.

The two-quasineutrons are distinguishable for the negative-parity states and thus the decoupling of the postive-parity and negative-parity quasiparticle can be investigated separately. The projection for each particle of $\vec{j}$ on the component of I in the $1-2$ plane, i.e., $j_\perp$, is plotted in Fig. 8. For $I \geq 4^-$ the positive-parity quasiparticle approaches a limiting value of $j_\perp^{(+)} \simeq 5.6$, which corresponds to almost complete alignment since $\langle j^{(+)}\rangle \simeq 6.0$. This positive-parity quasiparticle is predominantly $i_{13/2}$, for which the rotation-particle-coupling matrix elements are very large. The negative-parity quasineutron reaches a limiting value of $j_\perp^{(-)}$ for $I>10$, and the alignment is almost complete for odd I, i.e., $j_\perp^{(-)} \simeq 3.0$, and only partial for even I, i.e., $j_\perp^{(-)} \simeq 2.0$. Thus, the two quasineutrons of the negative-parity yrast states for odd spin are aligned to give a maximum $\langle J\rangle$ which is also aligned with $\vec{I}$ to maximum $J_\perp$, whereas the even-spin negative-parity yrast states have the j values coupled to $\langle J\rangle = J_{\max} - 1$ and with $\vec{J}$ again aligned with I.

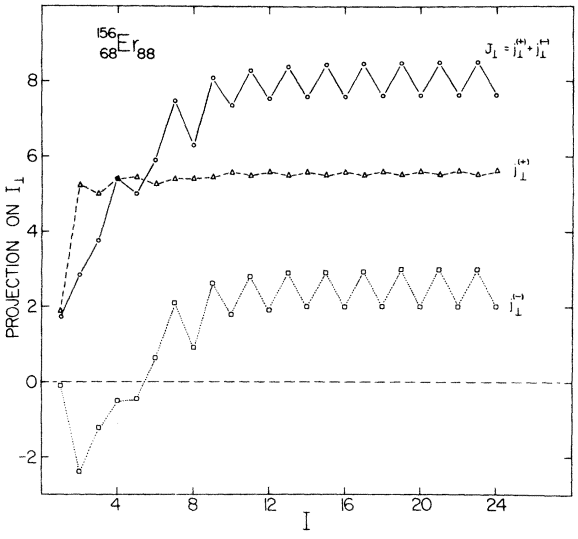

FIG. 8. Plot of $j_\perp^{(+)}$ and $j_\perp^{(-)}$, the projections of the individual intrinsic spins $\vec{j}$ on the component of $\vec{I}$ perpendicular to the symmetry axis for the yrast two-quasineutron bands in ^{156}Er.

C. $E\lambda$ transition strengths

The calculation of the electromagnetic transition rates and moments for the calculated two-quasiparticle states is quite straightforward if the wave functions are transformed into the $|IMRj_1j_2J\rangle$ basis described in Sec. II H. The process is quite lengthy, however, since a typical wave function may have up to 30 000 components in this basis. One can, nevertheless, make reasonable estimates based on the general features of the wave functions.

The $E1$ operator has no collective part; therefore, the transition rates are governed by $\Delta R = 0$ selection rule. In our case, we are interested in estimating the rates for decay of the odd-spin negative-parity to the even-spin positive-parity states, with $\Delta I = 1$. For such transitions, the difference between the mean R values is about 2.2 for the higher spin states. This greatly reduces the possibility of $\Delta R = 0$, resulting in a considerable inhibition of the rates from the single-particle estimates. This inhibition becomes stronger with increasing spin as R becomes purer. Only near the bottom of the bands would one expect noticeable interband $E1$ transitions.

The $E2$ rates can be estimated by neglecting the single-particle part of the $E2$ operator and by assuming a reasonably rotational behavior of the core. In such a case, the rates can be obtained in terms of the known $BE2$ from the first excited 2^+ state to the ground state by the formula:

$$\frac{B(E2;I_i \to I_f)}{B(E2;2_1^+ \to 0_1^+)} = \frac{\langle (R_i 020 \,|\, R_f 0)^2 \rangle}{(2020\,|\,00)^2} \, |\langle \chi_i \,|\, \chi_f \rangle|^2 , \qquad (19)$$

where $\langle \chi_i \,|\, \chi_f \rangle$ is the overlap of the intrinsic parts of the wave function of the initial and final states and $\langle (R_i 020 \,|\, R_f 0)^2 \rangle$ is an approximation to the expectation value of the square of the Clebsch-Gordan coefficient. The results of this procedure for the negative-parity yrast states are given in Fig. 9. The positions of the levels are shown schematically, and the $BE2$'s are given in multiples of $B(E2; 2_1^+ \to 0_1^+)$.

Three important conclusions can be derived from the above estimates. The first is that the odd-even splitting in the negative-parity yrast band is apparent not only in excitation energies, but also in the $BE2$ strengths. The rates within each subband (even or odd spin) are an order of magnitude larger than for the interconnecting transitions. Secondly, it is apparent that below the 7^- state the $E2$ strength is dissipated among

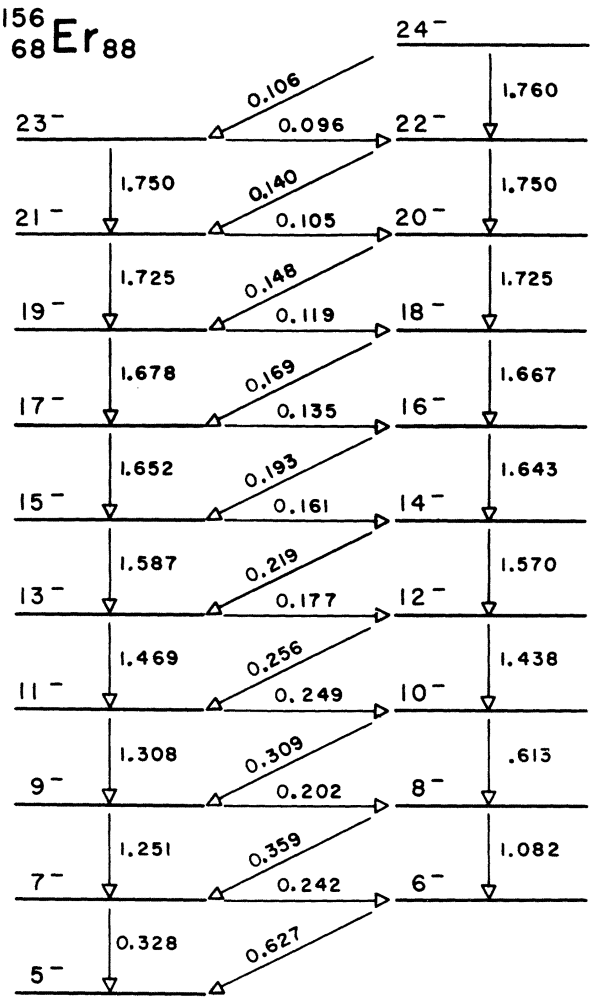

FIG. 9. Estimated $E2$ transition rates between two-quasineutron negative parity yrast states in ^{156}Er, in multiples of $B(E2; 2_1^+ \to 0_1^+)$.

several states, none being favored. This means that, experimentally, the odd-spin negative-parity band would appear to begin at the 7^- state, in agreement with the present data. The same is true, to a lesser extent, for the 10^- state in the even-spin case. The third and most significant observation is that, due to their excitation energies, the even-spin states have a finite decay branch ($\simeq$10%) to the odd-spin states and not vice versa. This would result in a much weaker population of the low-lying members of the even-spin negative-parity band compared to the odd-spin states, even if they are populated equally at high spin, explaining why the even-spin negative-parity states have not been observed. $M1$ transitions would similarly exhaust the even-spin states.

The situation is similar, but in reverse, for the positive-parity states. Here the odd-spin states become exhausted in favor of the even spins. In addition, the interband rates are stronger here, over 80% of the intraband rates (see overlaps in Table II), resulting in a much more dramatic depopulation of the unfavored odd-spin states.

It must be added that the above discussion applies not only to the yrast states but to the whole calculated high-spin two-quasiparticle spectrum which seems to separate into well defined bands, each with $\Delta I = 2$, a constant $\langle J \rangle$, and $J_\perp$, and with enhanced intraband $E2$ transition.

D. Magnetic dipole moments

The expectation values of the g factors of the calculated two-quasiparticle states are most easily estimated if the wave functions are expressed in the $|IMRj_1j_2J\rangle$ basis described in Sec. II H. The magnetic moment $\vec{\mu}$ can be expressed as

$$\vec{\mu} = g_I \vec{I} = g_J \vec{J} + g_R \vec{R} . \tag{20}$$

Using Landé's theorem and expanding J in terms of j_1 and j_2, one obtains

$$g_I(R,J,j_1,j_2) = \tfrac{1}{2}(g_J + g_R) + \frac{1}{2I(I+1)}(g_J - g_R) \times [J(J+1) - R(R+1)] ,$$

where

$$g_J(j_1,j_2) = \tfrac{1}{2}(g_{j_1} + g_{j_2}) + \frac{1}{2J(J+1)}(g_{j_1} - g_{j_2}) \times [j_1(j_1+1) - j_2(j_2+1)] . \tag{21}$$

Thus the only parameters needed to evaluate g_I are g_R, g_{j_1}, and g_{j_2}. The value for g_R can be taken to be the collective estimate

$$g_R = Z/A . \tag{22}$$

For g_j we have chosen the Schmidt limit values. The final calculated value for g_I becomes

$$g_I = \sum_{\substack{RJ \\ j_1 j_2}} |\langle IMRj_1j_2J | IM \rangle|^2 g_I(R,J,j_1,j_2) . \tag{23}$$

The overlap in Eq. (23) is given by Eq. (9).

The g factors calculated for some of the lower-lying bands in the two-quasineutron spectrum in ^{156}Er are shown in Fig. 10. One can observe a considerable deviation of the values of g_I from the collective estimate g_{ROTOR}. The values are strongly negative at low spins and slowly approach g_{ROTOR} with increasing spin. The yrast states seem to have the largest deviation from g_R, and some odd-even staggering is present.

The cause of this sharp lowering of g_I is relatively simple to understand. The single-particle g factors g_j for the $i_{13/2}$ neutrons are negative. Thus, for the states that have the intrinsic spin fully aligned with the rotation, the particle magnetic moment points in the opposite direction from the rotational magnetic moment. Near the onset of decoupling, most of the total spin is taken up by the particles, causing the particle magnetic moment to dominate. With increasing I, more and

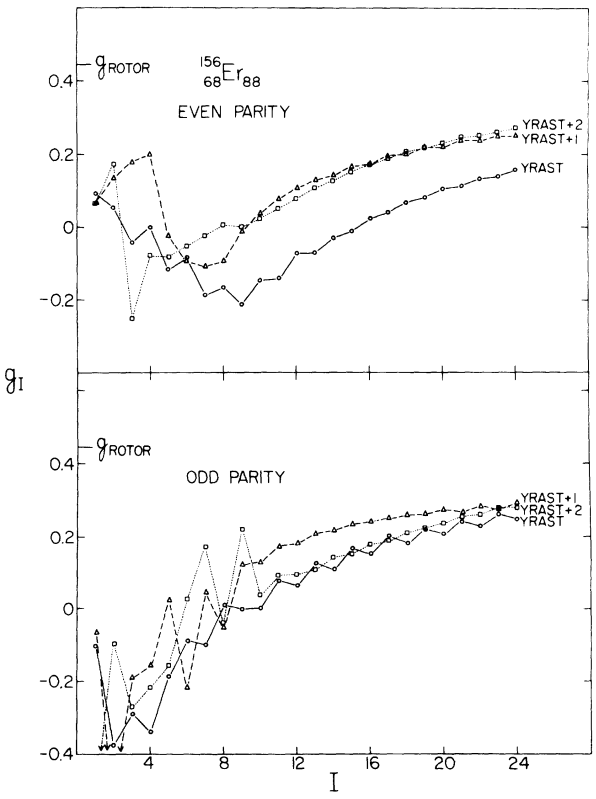

FIG. 10. Plot of the gyromagnetic ratio g_I versus I for some of the lowest two-quasineutron bands in ^{156}Er.

more spin is taken up by the rotation, forcing the magnetic moment to approach g_R.

It must be pointed out that the detailed calculation overestimates the deviation from g_R. Effective g_j are usually smaller in magnitude than their Schmidt limits. Thus, the g_j need not be as negative as the values used in the calculation, reducing the deviation from g_R. In addition, any mixing of the two-quasiparticle states with the zero-quasiparticle states would also tend to increase g_I, as the latter states are expected to have rotational magnetic moments. Nevertheless, the measurement of g_I in the region just above backbending for the even-parity states appears to be a crucial test of the model.

E. Effect of the residual interaction

It has been pointed out by Neergard, Vogel, and Radomski[25] that the residual two-body interaction may play an important role in producing the odd-even splitting in the negative-parity bands observed in the mercury nuclei. They have shown that after inclusion of a surface δ residual two-body interaction, modified by attenuating the higher multipoles to simulate a finite range, they were able to push the negative-spin states down in excitation energy, relative to the even-spin odd-parity states. They were unable to reproduce the experimental data with a pure rotational Hamiltonian. We therefore performed a calculation for ^{156}Er with the inclusion of the surface δ interaction in order to see what effect it would have on the yrast states. We used the strength G of 0.250 MeV and with no attenuation of the higher multipoles. The procedure is discussed in Sec. II F.

Two things can be said about the results even before the calculation is performed. One is that only the odd-I states are affected by this interaction for the negative-parity states, since $\pi + J$ in Eq. (8) must be even, and the odd- (even-) spin negative-parity states consist mainly of odd- (even-) J substates. Furthermore, since H_{SDI} is much smaller than H_R for $I > 10$, it will not affect significantly the wave functions of the states above spin 10. Then the only effect that the SDI would have on the negative-parity yrast states is a constant (downward for attractive force) shift of the odd-spin members. The exact calculation bears out the above conclusions. We found that the even-spin negative-parity yrast states between $I = 0^-$ and $I = 10^-$ are shifted down with the amount of shift varying from 63 keV for $I = 0^-$ to 22 keV for $I = 10^-$, while all the higher even-spin yrast states are shifted down by 13 keV. On the other hand, the yrast 1^- to 9^- odd-spin states were pushed down between 170 and 270 keV and the remaining odd-spin negative-parity yrast states were pushed down by amounts smoothly varying between 290 keV for 11^- and 315 keV for 23^-.

The effect on the positive-parity states was even less dramatic. Here mainly the even J are affected by the interaction, but since only the even J occur for both even- and odd-spin states, both would be affected in a similar way. In addition, a part of the strength for the even-spin states is expected to be taken away by the spurious states which should be excluded. Thus, although we find large downward shifts for the low-spin states, varying from 650 keV for the 0^+ to 70 keV for 10^+, above that spin the shifts for the even I decrease from about 40 keV for 12^+ to less than 10 keV for 24^+, and from about 125 keV for 11^+ to less than 60 keV for 23^+, for odd I. These shifts are quite small on the scale of the rotational energies.

A previous[26] interpretation of the odd-spin negative-parity states assumed them to be part of the $K = 0^-$ octupole band in order to explain the absence of the even-spin members. The rank-3 component of the residual two-body interaction will introduce octupole correlations into the negative-parity states if a sufficiently large configuration space is used. Switching on the residual interaction in the present calculation increased the $K = 0^-$ component in the wave function from 15% to 37% for the 3^- state, from 15% to 28% for the 5^- state, and by only 2% for odd-spin states with $I \geq 11^-$. The even-spin negative-parity states showed less than a 1% increase in $K = 0^-$ strength when the two-body force was included. The truncated configuration space used in the present calculations will attenuate the octupole correlations by about a factor of 2, which could be compensated for by using a stronger effective interaction. This will appreciably increase the octupole correlation for the lowest spin states but still be unimportant for states with $I \geq 11^-$. Thus, although the 3^-, 5^-, and 7^- states can be fairly well characterized as being members of the $K = 0^-$ octupole rotational band, the higher spin states, in this calculation, are essentially pure decoupled states, little influenced by octupole correlations. This is reasonable since the Coriolis decoupling matrix elements are much larger than the octupole correlation energies for $I \geq 11^-$. Obviously this rather sharp transition from octupole to decoupled structure will occur at a higher spin for nuclei where the Coriolis matrix elements are relatively smaller.

The present calculation indicates that the inclusion of the surface δ interaction does not significantly change the decoupling behavior for ^{156}Er

and appreciably influences only the relative excitation energies below the backbending region.

IV. APPLICATIONS TO OTHER NUCLEI

A. Other $N = 88$ nuclei

Since decoupling effects depend mainly on the position of the Fermi level, the results discussed in Sec. III can also be applied, with minor adjustments of parameters, to other $N = 88$ nuclei, such as ^{150}Sm, ^{152}Gd, ^{154}Dy, ^{158}Yb, etc. These nuclei would be expected to have decoupled two-quasineutron bands similar to those observed in ^{156}Er. Zolnowski and co-workers[27] have observed an odd-spin negative-parity band starting at 7^- in ^{152}Gd, and report having evidence of a similar band in ^{158}Yb. Similarly, Thompson, Johns, and Waddington[28] have seen a similar band up to spin 13^- in ^{150}Sm. This evidence supports the calculations presented in Sec. III.

B. Palladium nuclei

Our observation[10,29] of backbending and anomalous negative-parity bands in ^{126,128}Ba prompted us to perform the first calculation for barium nuclei. These calculations are described in a preliminary form in Ref. 10 and in a corrected and more detailed form in Ref. 29. The general features of the calculated spectra are similar to the ^{156}Er results, except that the anomalous behavior in ^{126}Ba is produced by the proton configurations. The observed[10,29,30] backbending behavior for the positive-parity states in ^{126,128}Ba and ^{128,130}Ce is reproduced and is caused by the decoupling of the two $h_{11/2}$ quasiproton configurations. The anomalous negative-parity bands, seen in ^{126,128}Ba are also well reproduced by configurations based on one decoupled $h_{11/2}$ quasiproton and a decoupled particle in the $g_{7/2}$ and $d_{5/2}$ orbitals. The calculated two-quasineutron states lie above the two-quasiproton states. However, the two-quasineu-

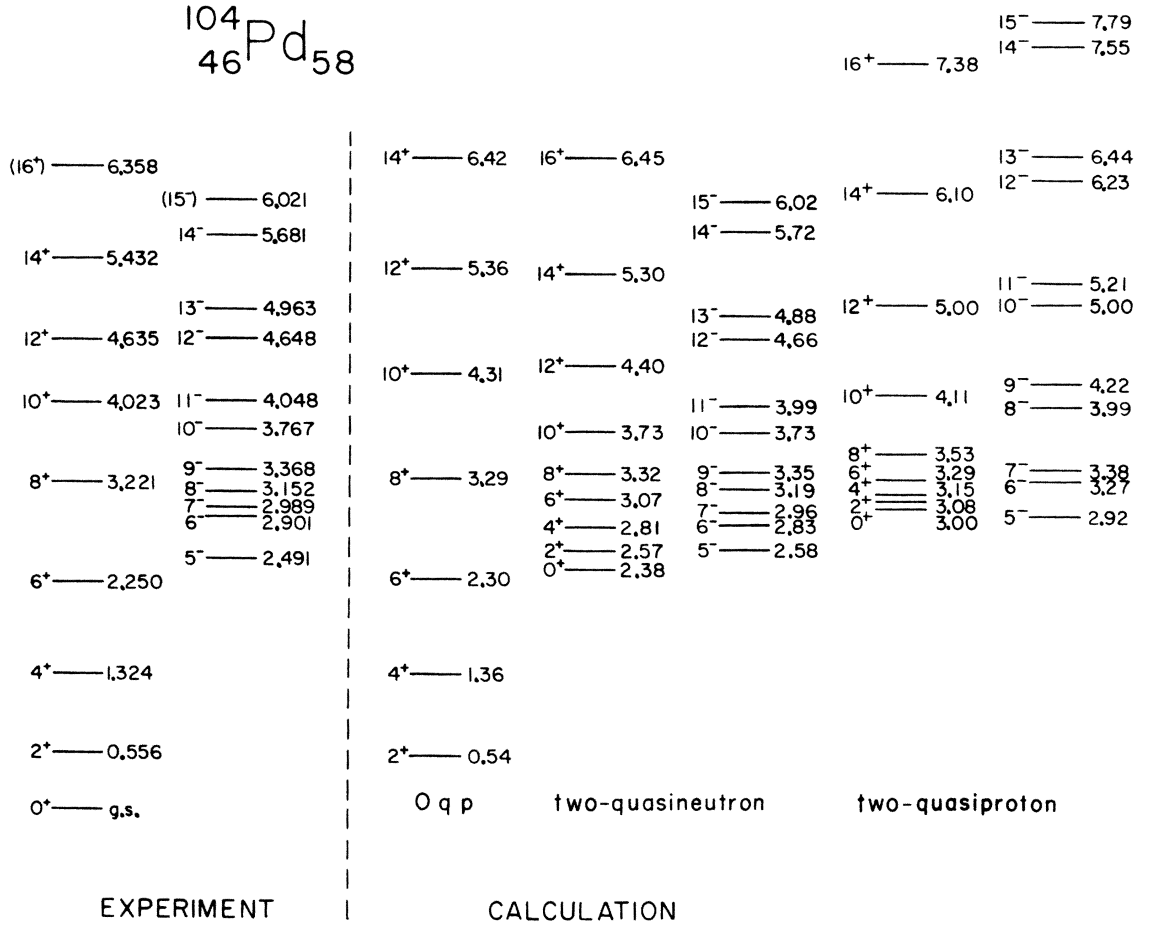

FIG. 11. Comparison of the calculated two-quasiparticle yrast states in ^{104}Pd with experiment.

tron states reproduce the observed isomeric 8^- states seen in several $N=74$ isotones[12,31,32] and similar states seen in the $Z=72$ and 74 proton analogs.[33]

The present model predicts that similar behavior to that seen for the proton states in ^{126,128}Ba should also occur near the $N=56$ neutron analogs. Such behavior, i.e., backbending and anomalous odd-parity bands, has been observed[13] in several Pd nuclei ($N=56$–60).

Calculation of two-quasiparticle states has been performed for the most extensively studied palladium nucleus[13] $^{104}_{46}\mathrm{Pd}_{58}$. The parameters are given in Table I. Palladium nuclei are soft to deformation and thus the moment of inertia of the zero-quasiparticle and two-quasiparticle bands was taken to be different.

The calculated spectrum is compared with the experimental results in Fig. 11. The yrast two-quasineutron states lie below the yrast two-quasiproton states, although they are fairly close in energy for low spin. The yrast two-quasiproton ($2q\pi$) and two-quasineutron ($2q\nu$) states exhibit decoupled bands for both positive and negative parity but the spacing between the decoupled two-quasiproton states is larger. This occurs because $\langle J\rangle_{2q\pi}\approx 6.5$ and $\langle J\rangle_{2q\nu}\approx 8.5$ resulting in $\langle R\rangle_{2q\pi} \simeq \langle R\rangle_{2q\nu}+2$. Thus the two-quasiproton states have more rotational energy for any given spin I.

Figure 11 illustrates that the two-quasineutron states reproduce remarkably well the experimental spectrum. In particular the odd-even splitting of the negative-parity band is in remarkable agreement with experiment. The close similarity in the calculated and experimental behavior in the vicinity of the $Z=N=56$ analogs is strong evidence supporting the present model.

V. CONCLUSIONS

Two-quasiparticle-plus-rotor bandmixing calculations have been performed to ascertain whether they can reproduce the phenomena of backbending and anomalous negative-parity bands which have been observed in even-A nuclei in several regions of the Periodic Table. The philosophy behind the present paper was to study the consequences of this model using reasonable parameters rather than forcing the parameters to best fit the data. In spite of this approach, these calculations reproduce the absolute excitation energies and known electromagnetic properties of the yrast bands seen in ^{104}Pd and ^{156}Er.

Detailed analysis of the eigenfunctions resulting from these calculations confirms the finding of Stephens and Simon[6] that a new coupling scheme emerges for high-spin two-quasiparticle states at intermediate deformation. In this coupling scheme the total intrinsic spin of the two decoupled quasiparticles J, and its projection on the component of the total spin perpendicular to the symmetry axis $J_\perp$, are fairly good quantum numbers. Well defined rotational bands are formed, each with its particular quantum numbers J, $J_\perp$; and the bands with maximum positive $J_\perp$ lie lowest in excitation energy, while the bands with maximum negative $J_\perp$ lie highest. In addition, when $|J_\perp|$ is maximal, that is, when the projections of the intrinsic spins on the symmetry axis are small, these bands will exhibit strong odd-even splitting. The lowest positive-parity decoupled two-quasiparticle band intersects the zero-quasiparticle band to form the yrast band above a critical spin, thus explaining the observed backbend within this model. The interaction matrix elements between these two bands have been shown to be remarkably small, i.e., $\leq$100 keV.

This model has two major limitations. The first is that the rotational Hamiltonian H_R may not necessarily be the dominant part of the total Hamiltonian for states in which the core rotation is small. Thus the inclusion of a realistic residual two-body interaction and extending the configuration space may have a large effect on the calculated states of low spin. The contribution of a reasonable residual two-body interaction has been shown to be unimportant for states with large $J_\perp$ (i.e., $J_\perp \sim J$), at high spin. The second limitation is that at very high spins all single-particle energies become insignificant, making it necessary to include a very large number of orbits in the calculation. Due to limitations on time and computer size, such calculations are difficult. On the other hand, it appears possible to perform calculations within the framework of this new coupling scheme. Such a calculation would be much more reliable for high-spin states.

It is evident that in order to obtain truly reliable representation of experimental spectra, it is necessary to perform more complete self-consistent calculations which take into account many-particle excitations and Coriolis antipairing. Calculations of the type performed by Banerjee, Mang, and Ring[7] or Faessler, Lin, and Wittman[8] show some hope of producing better results. Nevertheless, it is remarkable that such a simple model as the one described in this work can quantitatively explain many experimental phenomena.

Finally, we must emphasize the need for new and better experimental information. In particular, studies of electromagnetic properties, especially g factors, and searches for the unnatural-parity bands appear to be important tests of the model.

ACKNOWLEDGMENTS

The authors wish to thank Professor R. A. Sorensen and Professor P. Vogel for their invaluable comments and criticisms. An understanding of the interband interaction benefited greatly from discussions with Dr. F. S. Stephens, Dr. R. M. Diamond, and Dr. H. J. Mang.

---

†Supported by a grant from the National Science Foundation.

*Present address: Brookhaven National Laboratory, Upton, New York 11973.

[1]A. Johnson, H. Ryde, and J. Sztarkier, Phys. Lett. 34B, 605 (1971).

[2]A. Johnson and Z. Szymański, Phys. Rep. 7C, 182 (1973).

[3]R. A. Sorensen, Rev. Mod. Phys. 45, 353 (1973).

[4]F. S. Stephens, Rev. Mod. Phys. 47, 43 (1975).

[5]B. R. Mottelson and J. G. Valatin, Phys. Rev. Lett. 5, 511 (1960).

[6]F. S. Stephens and R. S. Simon, Nucl. Phys. A183, 257 (1972).

[7]B. Banerjee, H. J. Mang, and P. Ring, Nucl. Phys. A215, 366 (1973).

[8]A. Faessler, L. Lin, and F. Wittmann, Phys. Lett. 44B, 127 (1973).

[9]K. A. Hagemann, S. A. Hjorth, H. Ryde, and H. Ohlsson, Phys. Lett. 28B, 661 (1969).

[10]C. Flaum, D. Cline, A. W. Sunyar, and O. C. Kistner, Phys. Rev. Lett. 33, 973 (1974).

[11]L. L. Riedinger, G. J. Smith, P. H. Stelson, E. Eichler, G. B. Hagemann, D. C. Hensley, N. R. Johnson, R. L. Robinson, and R. O. Sayer, Phys. Rev. Lett. 33, 1346 (1974).

[12]H. Rotter, K. F. Alexander, C. Droste, T. Morek, W. Neubert, and S. Chojnacki, Nucl. Phys. A133, 648 (1969).

[13]J. A. Grau, Z. W. Grabowski, F. A. Rickey, P. C. Simms, and G. J. Smith, Bull. Am. Phys. Soc. 19, 1028 (1974); and private communication.

[14]A. W. Sunyar *et al.* (private communication).

[15]A. Bohr, K. Dan. Vidensk. Selsk. Mat.-Fys. Medd. 26, no. 14 (1952).

[16]B. E. Chi (private communication); Nucl. Phys. 83, 97 (1966).

[17]M. Baranger, Phys. Rev. 120, 957 (1960).

[18]C. J. Gallagher, Phys. Rev. 126, 1525 (1962).

[19]I. M. Green and S. A. Moszkowski, Phys. Rev. 139, B790 (1965).

[20]J. Högaasen-Feldman, Nucl. Phys. 28, 258 (1961).

[21]T. L. Khoo, F. M. Bernthal, J. S. Boyno, and R. A. Warner, Phys. Rev. Lett. 31, 1146 (1973).

[22]H. R. Andrews, D. Ward, R. L. Graham, and J. S. Geiger, Nucl. Phys. A219, 141 (1974).

[23]M. Piiparinen, J. C. Cunnane, P. J. Daly, C. L. Dors, F. M. Bernthal, and T. L. Khoo, Phys. Rev. Lett. 34, 1110 (1975).

[24]P. E. Nemirowski and Yu. V. Adamchuk, Nucl. Phys. 39, 551 (1962).

[25]K. Neergård, P. Vogel, and M. Radomski, Nucl. Phys. A238, 199 (1975).

[26]Y. Gono, D. R. Zolnowski, D. R. Heanni, and T. T. Sugihara, Phys. Lett. 49B, 338 (1974).

[27]D. R. Zolnowski, K. Kishimoto, Y. Gono, and T. T. Sugihara, Phys. Lett. 55B, 453 (1975).

[28]J. V. Thompson, M. W. Johns, and J. C. Waddington, Can. J. Phys. 53, 1229 (1975).

[29]C. Flaum, D. Cline, A. W. Sunyar, O. C. Kistner, Y. K. Lee, and J. S. Kim, Nucl. Phys. (to be published).

[30]W. Dehnhardt, S. J. Mills, M. Müller-Veggian, U. Neumann, D. Pelte, G. Poggi, B. Povh, and P. Taras, Nucl. Phys. A225, 1 (1974).

[31]D. Ward, R. M. Diamond, and F. S. Stephens, Nucl. Phys. 117, 309 (1968).

[32]R. A. Warner and J. E. Draper, Phys. Rev. C 1, 1069 (1970).

[33]*Table of Isotopes*, edited by C. M. Lederer *et al.* (Wiley, New York, 1967), 6th ed., and references contained therein.